



Research Article

**FACILE SYNTHESIS OF  $\gamma$ -ALUMINA NANOPARTICLES VIA THE SOL-GEL METHOD IN PRESENCE OF VARIOUS SOLVENTS**

**Seyed Mahdi SIAHPOOSH<sup>1</sup>, Esmacel SALAHI<sup>2\*</sup>, Fereidoun Alikhani HESSARI<sup>3</sup>, Iman MOBASHERPOUR<sup>4</sup>**

<sup>1</sup>Materials and Energy Research Center (MERC), Tehran, IRAN

<sup>2</sup>Materials and Energy Research Center (MERC), Tehran, IRAN

<sup>3</sup>Materials and Energy Research Center (MERC), Tehran, IRAN

<sup>4</sup>Materials and Energy Research Center (MERC), Tehran, IRAN

**Received: 10.03.2017 Revised: 17.05.2017 Accepted: 11.07.2017**

**ABSTRACT**

In present investigation,  $\gamma$ -alumina nanoparticles with less than 10 nm sizes and high surface area was prepared using sol-gel method in presence of aluminum isopropoxide as an aluminum precursor, distilled water, acetic acid as hydrolysis rate controller and 1-butanol, tert-butanol and 2-propanol as solvent. The effects of solvent type on textural properties of the as-received and heat treated  $\gamma$ -alumina were investigated.

The received powder was characterized by simultaneous thermal analysis (DTA/TGA) method. The calcined  $\gamma$ -alumina nanoparticles were characterized using X-Ray diffractometer (XRD), field emission scanning electron microscopy (FESEM), fourier transform infrared spectroscopy (FTIR) and nitrogen adsorption-desorption techniques.

This study revealed that the solvent types, weight ratios of reactants, calcination temperature and time were important factors to preparation of  $\gamma$ -alumina with high surface area (in the range of 339–351 m<sup>2</sup>/g) and relatively narrow pore size distribution.

**Keywords:**  $\gamma$ -alumina, nanoparticles, sol-gel, aluminum isopropoxide, solvent.

**1. INTRODUCTION**

Powder preparation is a great important step in ceramic processing [1]. Non-traditional methods have advantages and disadvantages according to their nature. They are divided into three main classes which consist of solution, vapor phase and salt decomposition.

In present study, sol-gel method was used for preparation of  $\gamma$ -alumina nanoparticles. Despite presence of many researches about synthesis of mesoporous  $\gamma$ -alumina, it is still a challenge to develop a facile and surfactant-free solution route for preparation of these materials using non-traditional methods.

Properties of alumina are largely dependent on properties of boehmite, so to obtain expected alumina materials, many efforts have been done to preparation of boehmite with different morphologies and microstructures.

\* Corresponding Author/Sorumlu Yazar: e-mail/e-ileti: e-salahi@merc.ac.ir, tel: (+98) 261 6204131 / 912 1500168

G. Jian-feng *et al.*, [2] and S.C. Shen *et al.*, [3] used the precursor of aluminum nitrate and in another research D. Ma *et al.*, [4] used aluminum chloride precursor and produced  $\gamma$ -alumina nanoparticles through the hydrothermal method, the main limitation for them being lack of high-purity powder. J. Mullens *et al.*, [5] prepared boehmite and  $\gamma$ -alumina platy nanoparticles with the same method, using aluminum alkoxide precursor and achieved particles with high purity and low levels of agglomeration in the range of 30-80 nm. In another study Y. Zhai [6] examined making the  $\gamma$ -alumina by ethanol precipitation, results indicated that ethanol would prevent from creation of agglomerates in the deposition.

M.G. Ma *et al.*, [7] and Y.J. Zhu *et al.*, [8], prepared  $\gamma$ -alumina powder as a bundle-like and rod-like morphology, respectively, using solvothermal method and with the precursor of aluminum chloride. H.V. Fajardo *et al.*, [9] and T.C. Haung *et al.*, [10] prepared mesoporous alumina spheres and  $\gamma$ -alumina membranes using sol-gel method, respectively. M. Vallet-Regí *et al.*, [11] used the spray pyrolysis method and Z. Károly and J. Szépvölgyi [12] used thermal plasma to obtain hollow alumina spheres with diameter less than 100  $\mu\text{m}$ .

M. Chatterjee *et al.*, [13] illustrated crystallization of  $\gamma\text{-Al}_2\text{O}_3$  at 378°C and crystallization of chain-like pure  $\alpha\text{-Al}_2\text{O}_3$  with low surface area at 800°C by the sol-emulsion-gel method under simultaneous mechanical agitation. H.C. Zeng *et al.*, [14], produced mesoporous alumina, with high specific surface area using the precursor of tri-sec-butoxide aluminum. By the similar raw material, J. Valente *et al.*, [15] produced  $\gamma$ -alumina and K.W. Jun *et al.*, [16] prepared the  $\gamma$ -alumina activated by silica and B.F. Woodfield *et al.*, [17] synthesized the mesoporous  $\gamma$ -alumina. Also, H. Dabbagh *et al.*, [18] used the alanine amino acid for the first time as a gel maker to prepare  $\gamma$ -alumina. J. Fernandes *et al.*, [19] and M. Sasani Ghamsari *et al.*, [20] reduced the cost of raw materials and prepared mesoporous  $\gamma$ -alumina with the sol-gel method using aluminum nitrate and aluminum chloride, respectively. M. Rezaei *et al.*, [21] produced nanocrystalline  $\gamma$ -alumina with sucrose surfactants and showed an increase in specific surface area and reduction in particle size of the resultant  $\gamma$ -alumina. However, Y. Liu *et al.*, [22] did not use surfactants due to thermal instability, environmental risks and high price in the preparation of  $\gamma$ -alumina.

According to the researches, the final product of the sol-gel method has high purity and surface energy. The way of doing the process and achieving small sized particles is by using solution conditions and having low temperature during heat treatment [23]. On the other hand, even though aluminum isopropoxide precursor is not completely soluble in ethanol [5], it is the most commonly-used solvent for the preparation of  $\gamma$ -alumina nanoparticles via the sol-gel method. The effects of other solvents on the textural and morphological properties of  $\gamma$ -alumina in the presence of this precursor and acidic catalyst have not been studied thoroughly.

So, the sol-gel method is used in this research for preparation of  $\gamma$ -alumina nanoparticles with specific surface area higher than 300  $\text{m}^2/\text{g}$ , high pore volume and well defined narrow pore size distribution for heavy metals adsorption. The different solvents effects were also investigated on the textural and structural properties of synthesized  $\gamma$ -alumina. This work was also emphasized on using almost cheap raw materials with accepted level of purity.

## 2. EXPERIMENTAL PROCEDURES

### 2.1. Starting materials

Preparation of  $\gamma$ -alumina nanoparticles was done by the sol-gel method with cheap and high purity raw materials and without environmental pollution. Aluminum isopropoxide alkoxide as aluminum precursor instead of aluminum inorganic salts produces  $\gamma$ -alumina powder with a higher specific surface area. This material is cheaper and easily available compared to many other alkoxides such as tri-sec-butoxide aluminum. Aluminum isopropoxide (AIP,  $\text{Al}(\text{OCH}(\text{CH}_3)\text{CH}_2)_3$ , >98.0% wt%, MERCK Art. No. 801079), 1-butanol ( $\text{CH}_3(\text{CH}_2)_3\text{OH}$ , >99.5% wt%, MERCK Art. No. 988), tert-butanol ( $(\text{CH}_3)_3\text{COH}$ , >99.0% wt%, MERCK Art. No. 822264), 2-propanol

( $\text{CH}_3\text{CH}(\text{OH})\text{CH}_3$ , >99.0% wt%, MERCK Art. No. 995) and acetic acid (AA,  $\text{CH}_3\text{CO}(\text{OH})$ , >63.0% wt%, MERCK Art. No. 62) were used as starting materials. In all the preparation stages, distilled water was used.

## 2.2. Synthesis of $\gamma$ -alumina

All experiments were conducted under air. Aluminum isopropoxide was used as aluminum precursor, acetic acid as hydrolysis rate controller and 1-butanol, tert-butanol and 2-propanol as solvent, during synthesis procedure. The weight ratios of reactants AIP: Solvent, AIP:  $\text{H}_2\text{O}$ , and AIP: AA were 1:60, 1:1, and 40:1, respectively. Initially, 3g of AIP was separately dissolved in 222 ml, 230.8 ml and 229 ml of 1-butanol, tert-butanol and 2-propanol, respectively, and AIP solution was prepared under continuous and vigorous magnetic stirring for 3 hours until all AIP particles dissolved at room temperature. Then, the mixture of 0.07 ml acetic acid and 3ml distilled water was added drop-wise into the above solution. The solution was magnetically stirred for 3 hours for completion of hydrolysis. During the reaction, the solution was stirred at 150 rpm and formed a uniform product.

After adding the two solutions, the final solution was placed in a glass vessel at room temperature for 24 hours and resulted in formation of a gel. The gel was dried in an oven at  $120^\circ\text{C}$  for 6 hours in flow of air. A white dry gel was obtained, which was pulverized and passed through 70-mesh sieve for the next test.

Heat treatment for powder calcination took place in a normal environment, using a laboratory chamber furnace with ability to reach  $1500^\circ\text{C}$  maximum temperature. The sample was poured in an alumina crucible and heated to  $600^\circ\text{C}$  with ramp rate of  $2^\circ\text{C}/\text{minute}$ . It was maintained in that temperature for 6 hours so that  $\gamma$ -alumina white powder was obtained after slow and gradual cooling in the furnace.

In the present study, the samples were labeled as Ab, At and Ap where A represents alumina and b, t and p, represent the 1-butanol, tert-butanol and 2-propanol solvent, respectively. To complete the study, resulted analysis of prepared samples were compared with commercial  $\gamma$ -alumina sample with Ac ID also.

## 2.3. Characterization

Proper temperature for calcination process of the dried sample was determined using the differential thermal and thermogravimetric analysis instrument (BÄHR, STA-503, Germany).

Phase identification and crystallinity of the sample were done by X-Ray diffraction (XRD) using Siemens D-500, semi-automatic, at room temperature with  $\text{CuK}\alpha$  radiation. It is noteworthy that  $\text{CuK}\alpha$  radiation was obtained from a copper X-Ray tube operated at 30 kV and 25 mA ( $\lambda=1.5404 \text{ \AA}$ ). Also, the particle size was estimated using Scherer equation in nanometer [24].

The specific surface area, the total pore volume, and the distribution of pore diameter of the calcined samples were measured using nitrogen gas adsorption/desorption isotherm at liquid nitrogen temperature (77.4K) and a Belsorp instrument (mini-II version). Specific surface areas were calculated using the Brunauer-Emmett-Teller (BET) equation, at  $P/P_0$  range between 0.05-0.35. It should be noted that P and  $P_0$  are partial pressure in the adsorbed gas by Pascal in equilibrium and experimental conditions, respectively. Assuming sphericity and same size of the particles, the measured specific surface area for samples in crystallite forms were converted to equivalent particle size according to the equation (1) [25]:

$$D_{\text{BET}} = \frac{6000}{\rho \cdot S_{\text{BET}}} \quad (1)$$

where  $D_{\text{BET}}$  is average particle size by nm,  $S_{\text{BET}}$  is specific surface area expressed in  $\text{m}^2/\text{g}$  and  $\rho$  the theoretical density expressed in  $\text{g}/\text{cm}^3$ .

Pore size distribution of sample was obtained employing the Barrett-Joyner-Hatenda (BJH) model.

The field emission scanning electron microscopy (FESEM) images were obtained with a TESCAN-MIRA3 scanning microscope operated at an acceleration voltage of 10 kV and used to study the surface of the sample. To determine the elements in sample, the energy dispersive X-Ray spectroscopy (EDS) was used for prepared powders using microscope ancillary facilities.

Fourier transform infrared spectroscopy (FTIR) is an important tool in the identification of functional groups that may be present in different substances. FTIR spectra of dispersed samples on KBr disks were recorded at room temperature using Perkin Elmer spectrometer (Spectrum 400, United States) in the range of 4000 to 400  $\text{cm}^{-1}$  at a resolution of 4  $\text{cm}^{-1}$  and 30 scans for each run. Disks were dried at 373K for 24 hours prior to recording the FTIR spectrum.

### 3. RESULTS AND DISCUSSION

#### 3.1. Thermal analysis

DTA/TGA profiles for alumina precursors provide insights into the phase transition from boehmite to  $\gamma$ -alumina. The DTA/TGA curves of as-dried boehmite precursor according to presence of tert-butanol as solvent and acetic acid as hydrolysis controller, during processing are shown in figure 1.

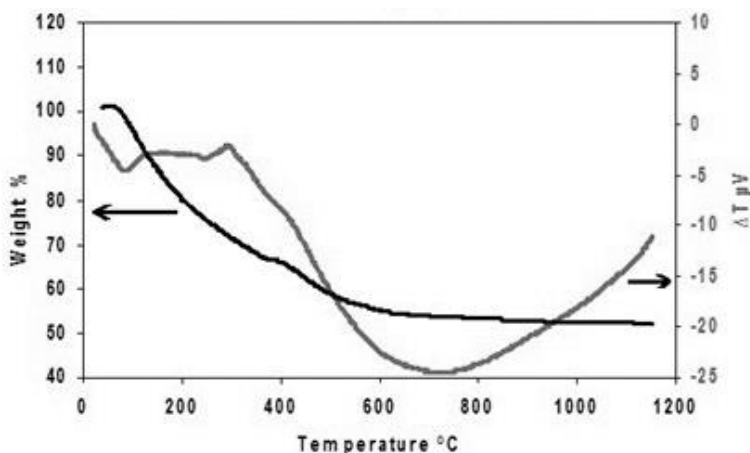


**Figure 1.** DTA/TGA curves of the as-dried boehmite precursor

The DTA curve presents three major peaks among which two of them are endothermic and the main peak is exothermic. In light of the as-dried boehmite precursor TGA curve, it seems that there are three stages of decomposition reaction with a total weight loss of ~45%. The initial stage corresponds to an endothermic weight loss of ~20% which is attributable to the remove of physically adsorbed water and residual moisture from room temperature to 200°C. The second weight loss, between 200°C to 500°C is an exothermic process that occurred due to the decomposition of organics including adsorbed acetic acid and the removal of chemically adsorbed water molecules. It should be noted that the decomposition temperature of acetic acid is about 440°C. The third stage comes with appearance of exothermic broad peak has been happened above 500°C which is attributable to a weight loss due to the crystallization of transition alumina, oxidation of organic volatile residues, elimination of OH groups and slow continuous dehydroxylation. The total weight loss in last two stages is ~25%. A continuously falling TGA

curve suggests that a slow dehydroxylation reaction proceeds as a function of temperature. TGA curve is flat at temperatures of about 600°C and it can be seen no significant weight loss at higher temperatures, meaning that the organic residues have been removed completely and the sample has reached to a stable structure. Therefore, it is suitable to perform the calcination process at temperature of about 600°C.

### **3.2. X-Ray diffraction**

The crystalline nature of commercial  $\gamma$ -Al<sub>2</sub>O<sub>3</sub> and prepared samples with aluminum isopropoxide in alcoholic solvents of 1-butanol, tert-butanol and 2-propanol was studied by X-Ray diffraction. All prepared samples were calcined for 6h at 600°C in air. The results in high-angle diffraction is shown in figure 2. It can be found that the resulted patterns at high diffraction angles are nearly similar and the percentages of samples crystallinity do not differ significantly. The three main reflections of  $\gamma$ -Al<sub>2</sub>O<sub>3</sub> phase are clearly observed as broad peaks at 2 $\theta$  angles around 37°, 46°, and 66° which correspond to (311), (400), and (440) planes, respectively, according to JCPDS PDF No. 001-1308. Diffraction peaks observed in XRD patterns were broad because crystallites were very small. Such sizes indicate their partly weak crystalline nature in the prepared and commercial  $\gamma$ -alumina. It should be noted that no peak of other phases of alumina is recognizable in diffraction pattern of prepared samples and  $\gamma$ -alumina phase is the only detectable phase. Nevertheless, in addition to three main reflections of  $\gamma$ -alumina phase in mentioned angles, other peaks are seen in X-Ray diffraction of commercial sample that probably related to the presence of other transitional alumina phases, or entering impurities to composition in manufacturing process.

The calculation is done for commercial and prepared  $\gamma$ -alumina based on Scherrer equation in (440) planes with the maximum intensity of diffraction and 2 $\theta$  angle of 66°. The average crystallite sizes ( $D_{XRD}$ ) of commercial sample obtained is 8.4 nm and for Ab, At and Ap prepares powders obtained are 5.5, 5.4 and 5.6 nm, respectively, which represents the nanometer structure. The results imply that the average crystallite size of the prepared powder samples with different solvents is almost in the same range of about 5 nm and is smaller compared with the commercial sample.

### **3.3. Textural properties**

Textural properties consist of the total pore volume, specific surface area and average particle size of commercial  $\gamma$ -alumina and the  $\gamma$ -alumina prepared with sol-gel method using aluminum isopropoxide in presence of mentioned solvents and acetic acid catalyst are presented in table 1.

The results show that the sol-gel derived  $\gamma$ -alumina nanoparticles have more specific surface area than commercial  $\gamma$ -alumina.

It is noteworthy that maximum surface area of 351 m<sup>2</sup>/g is obtained when tert-butanol is used as solvent. This proves that textural properties are influenced by the type of used solvent, and this sample has the smallest particle size between all samples.

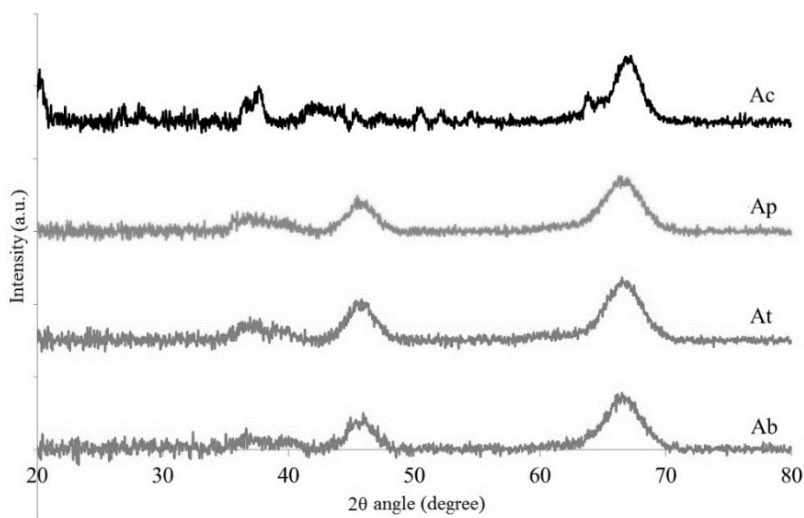


**Figure 2.** X-Ray diffraction pattern at high angles diffraction for commercial and prepared samples

**Table 1.** Selected textural properties of commercial and prepared  $\gamma$ -alumina

Sample ID	Specific surface area (m <sup>2</sup> /g)	Pore volume (cm <sup>3</sup> /g)	Average particle size (nm)
Ab	343	0.887	5.46
At	351	1.09	5.34
Ap	339	1.29	5.53
Ac	306	0.226	6.13

According to table 2, the specific surface area and pore volume of prepared  $\gamma$ -alumina nanoparticles in present study is relatively higher than the previous researches.

**Table 2.** Selected textural properties of prepared  $\gamma$ -alumina via different methods in the previous researches

Method	Precursor	Specific surface area (m <sup>2</sup> /g)	Pore volume (cm <sup>3</sup> /g)	Reference
solvent-deficient	tri-sec-butoxide aluminum	100	0.56	[26]
thermal decomposition	ammonium aluminum carbonate hydroxide	263	0.64	[27]
thermal decomposition	boehmite	192	0.44	[21]
precipitation	aluminum chloride	177	0.41	[28]
precipitation	aluminum nitrate	190	0.46	[29]
solvothermal	aluminum nitrate	216.7	1.06	[22]
sol-gel	aluminum nitrate	246	0.25	[20]
sol-gel	phosphide aluminum	285		[30]
sol-gel	aluminum isopropoxide	257	0.89	[31]

The nitrogen adsorption/desorption isotherms of commercial and sol-gel derived samples are shown in figure 3. According to IUPAC classification, the obtained isotherms for Ab and Ac samples are characterized as IV type and for other samples are V type. Contrast to commercial

sample, prepared samples isotherms have been extended in almost flat and stretched condition until reach high relative pressures, which is the characteristic of solids with meso porosity. In addition, the significant slope change occurs in the curve at high relative pressures of about  $P/P_0=0.9$ , which indicates presence of some macro pores in the structure of the sol-gel derived samples. The shape of the hysteresis loops can be correlated with the change in pore structure, which in this case can be a phase transformation from boehmite to  $\gamma$ -alumina with different morphologies [32]. In this study hysteresis loops for all prepared samples occurred at a relative pressure range of  $P/P_0=0.4-0.98$ . They are H1 type that adsorption and desorption branches have parallel mode completely, so most of the pores are in cylindrical shape. Hysteresis loop of commercial sample is in the range of  $P/P_0=0.4-0.98$  and H2 type that confirms formation of layer structure. The porosity volume in the prepared samples is relatively higher than the previous researches [25, 33 and 34] and the commercial sample, is confirmed with the ultimate amount of absorbed nitrogen by the samples. So that amounts are more than  $600 \text{ cm}^3/\text{g}$  for prepared samples, indicating presence of large volume pores, while that is less than  $150 \text{ cm}^3/\text{g}$  in commercial sample.

Figure 4 shows pore-size distribution of commercial and prepared samples employing BJH model. They indicate on relatively narrow distribution of micro and mesopores with 1-10 nanometer sizes in Ab, At and Ap samples, where related maximum peak is seen in 2.7, 2.1 and 2.1 nm, respectively. Based on the research done, there is a narrow pore-size distribution in the range of 1 to 10 nm of interest for both adsorption and catalytic applications [32]. Accordingly, it appears that commercial  $\gamma$ -alumina, according to the figure 4-d, is not suitable case for these applications, due to more pores of this sample have a size of less than 2nm. The obtained results indicate that Ab sample has narrower pore size distribution and smaller average pore diameter comparing with other prepared samples.

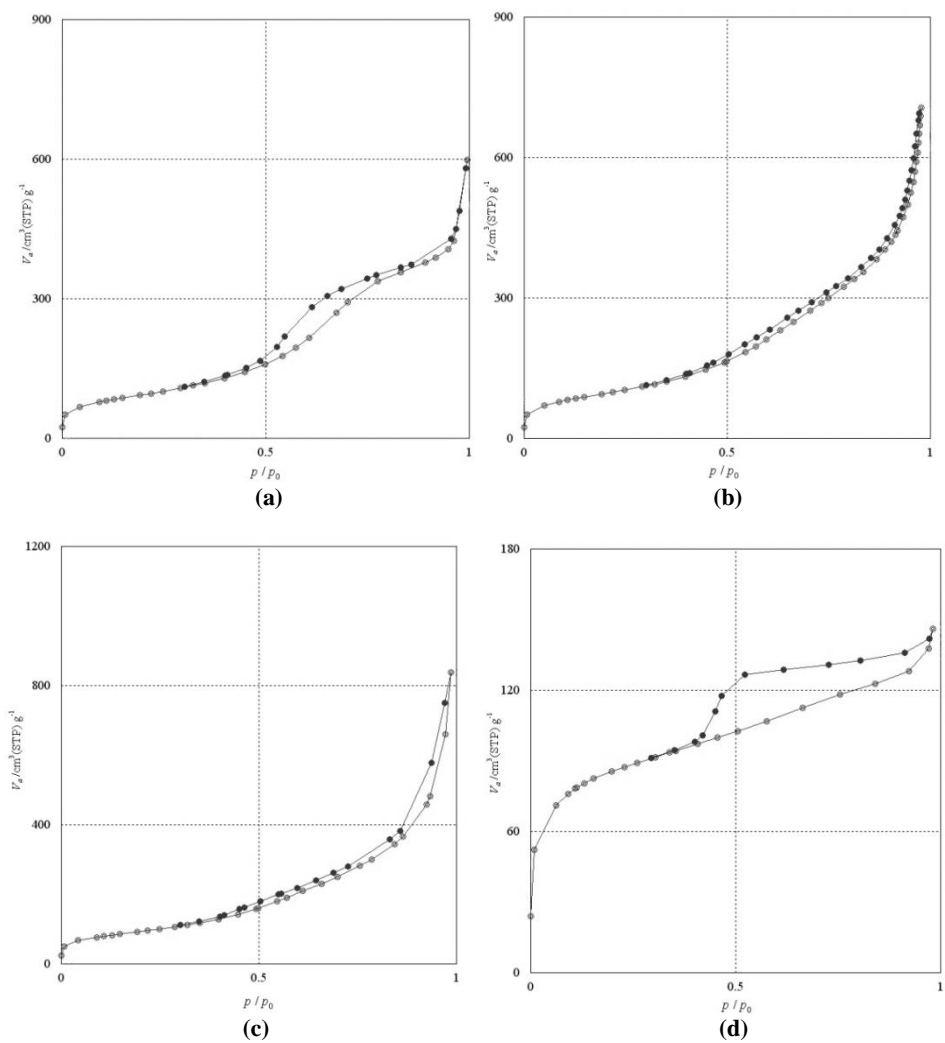


**Figure 3.** Nitrogen adsorption/desorption isotherms for samples: a) Ab, b) At, c) Ap and d) Ac

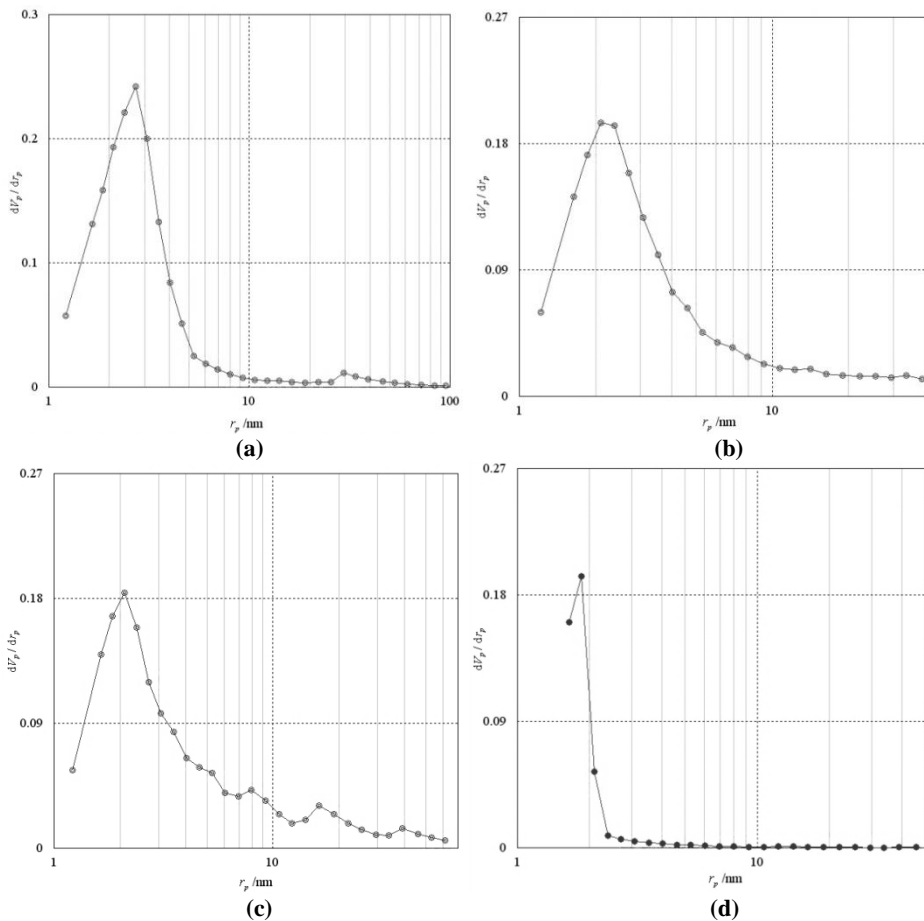


**Figure 4.** BJH model of samples: a) Ab, b) At, c) Ap and d) Ac

It is evident that by varying the used solvents in the process,  $\gamma$ -aluminas is provided with relatively high surface area, large pore volume and suitable pore size distribution which is desirable for heavy metal adsorption. The results show that the length of alkyl chain of used alcohol as solvent plays a key role in the formation of such architectures, so the pore diameter increases with increasing chain length of the alcohol [32].

The relationship between solvent surface tension and capillary pressure is represented in equation (2).  $\Delta P$  represents the capillary pressure,  $\gamma$  is the surface tension,  $\theta$  is the contact angle between the solvent and the pore wall, and  $r$  is the average pore radius.

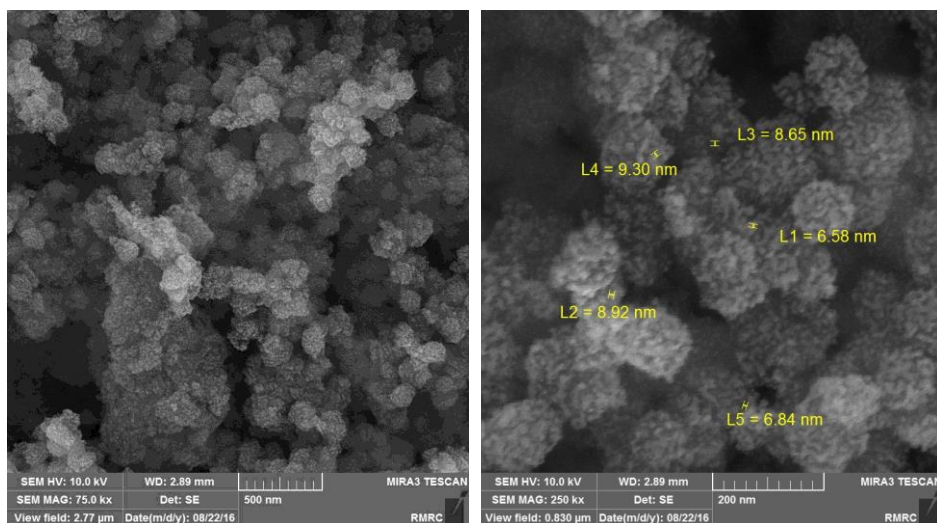
$$\Delta P = \frac{2\gamma \cos \theta}{r} \tag{2}$$

According to this equation, higher surface tension of solvent, results in higher capillary pressure inside the pores which leads to more pore shrinkage during the solvent removal step, and eventually results in a calcined product with lower pore volume. This behavior may explain the lower pore volume for Ab which 1-butanol has higher surface tension compared with all alcoholic solvents in study, according table 1.

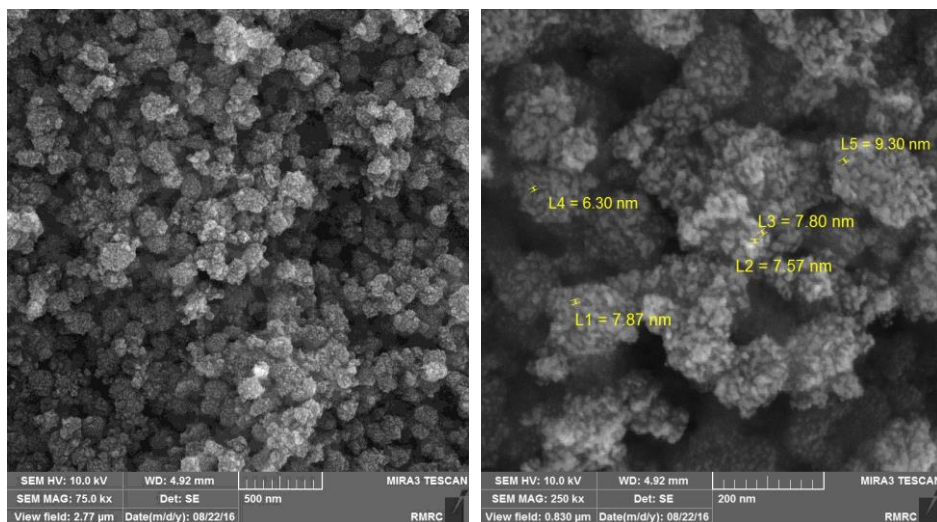
### 3.4. Morphology

Figures 5 and 6 show FESEM images and the diagram obtained from EDS analysis of the prepared  $\gamma$ -alumina nanoparticles, respectively. As shown, the samples have spongy structure and are composed of porous and homogenous aggregates with different sizes. These aggregates have nanoparticles with less than 10 nm size. The results are in accordance with the particle sizes which were estimated by BET data.

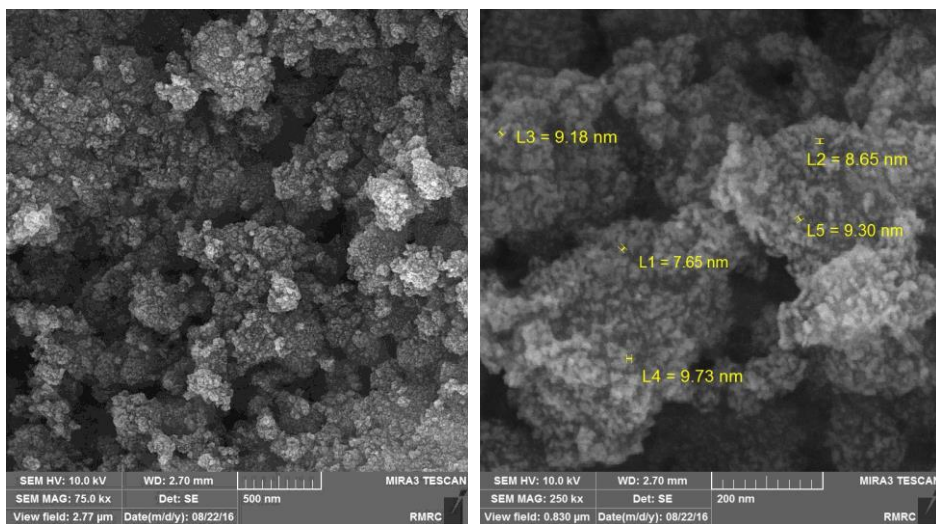
EDS analysis results confirmed presence of aluminum and oxygen ions. It is noteworthy that presence of carbon and gold peaks were related to the substrate of carbon and used metal for analysed powder coating, respectively.



(a)

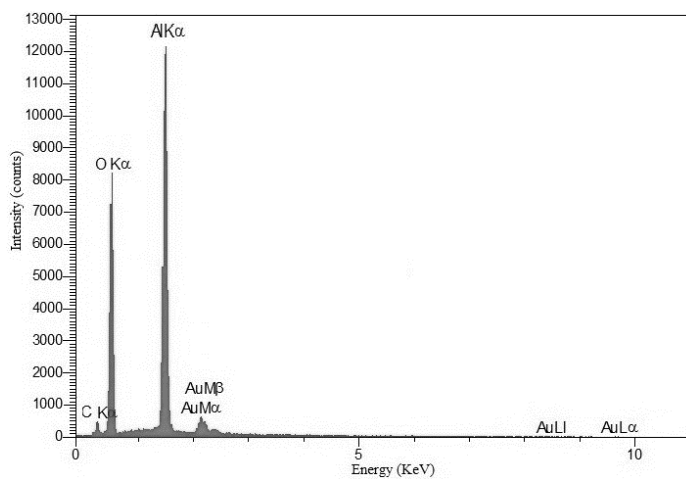


(b)



(c)

Figure 5. SEM image of samples: a) Ab, b) At and c) Ap



(a)

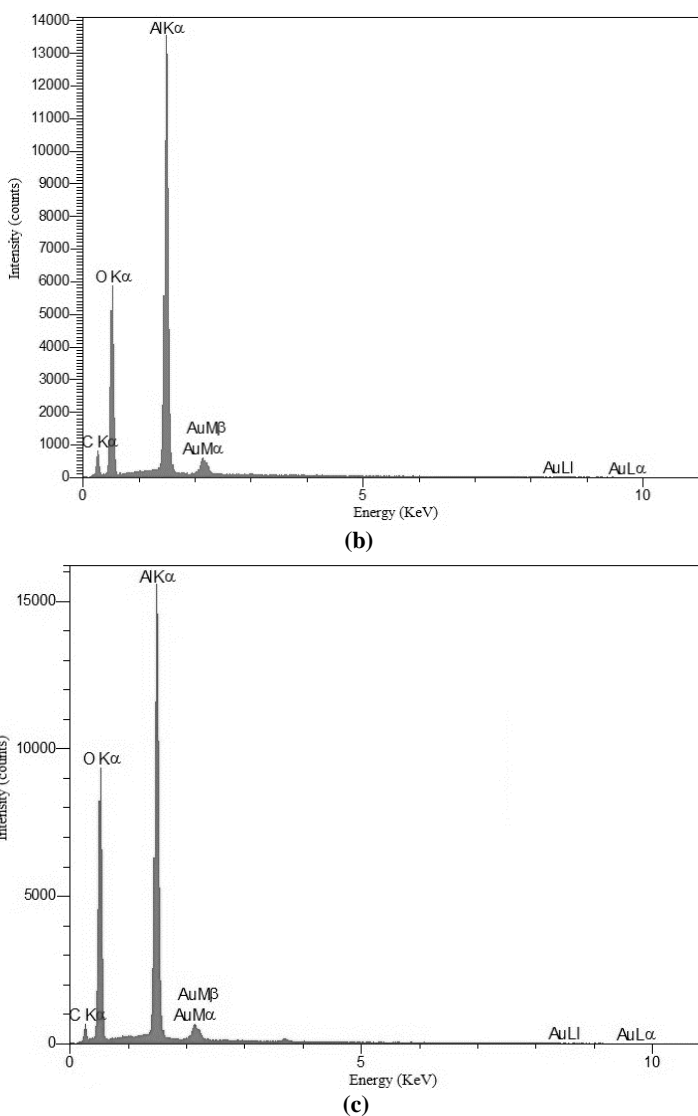


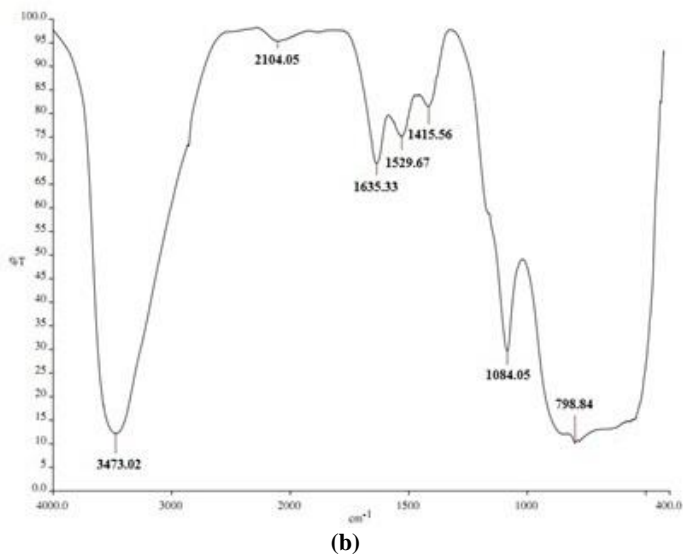
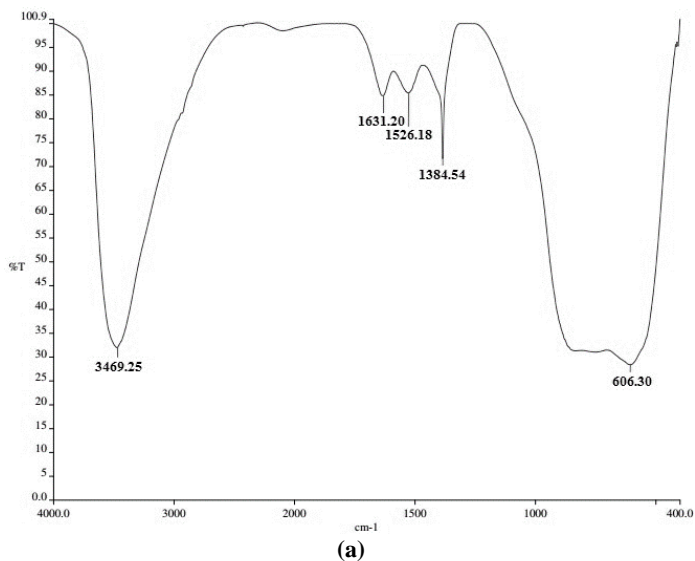
**Figure 6.** EDS diagram of samples: a) Ab, b) At and c) Ap

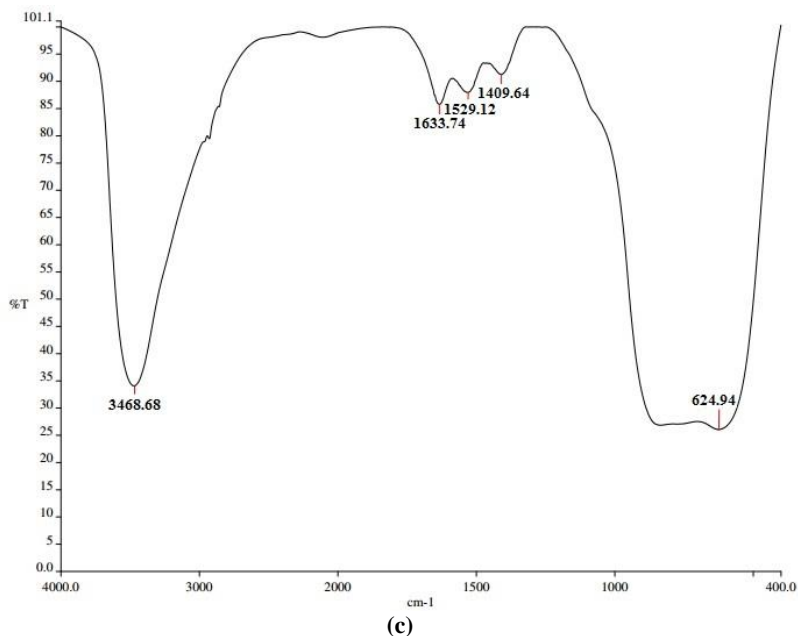
### 3.5. Fourier transformation infrared spectroscopy

Figure 7 shows the FTIR spectra for the Ab, At and Ap samples recorded in KBr pellet. The strong broadening band at  $3800\text{--}3000\text{ cm}^{-1}$  occurs due to the hydrogen bond between the various hydroxyl groups in prepared  $\gamma$ -alumina nanoparticles.

Another broadening band, which existed at  $1000\text{--}400\text{ cm}^{-1}$ , corresponds to Al–O vibration. The broad –OH stretching adsorption band, which appeared at  $3469.25\text{ cm}^{-1}$ ,  $3473.02\text{ cm}^{-1}$  and  $3468.68\text{ cm}^{-1}$  in Ab, At and Ap samples, respectively, reveal the presence of hydroxyl groups. The weak peak at  $1631.20\text{ cm}^{-1}$ ,  $1635.33\text{ cm}^{-1}$  and  $1633.74\text{ cm}^{-1}$  in Ab, At and Ap samples,

respectively, relate to the bending mode of adsorbed water. Peaks in the range of 1600–1400  $\text{cm}^{-1}$  belong to  $-\text{OH}$  group's vibrations and impurities. The broad adsorption band at 798.84  $\text{cm}^{-1}$  in the At sample shows  $\text{AlO}_4$  stretching mode and the peak in range of 700–500  $\text{cm}^{-1}$  in prepared  $\gamma$ -alumina nanoparticles relates to the  $\text{AlO}_6$  stretching mode. So At sample has both tetrahedral and octahedral conditions. It is also expected that  $\text{Al}-\text{O}-\text{H}$  bending mode be in range of 1200–900  $\text{cm}^{-1}$ . It is seen that there is a strong peak at 1084.05  $\text{cm}^{-1}$  in the At sample and a small hump at about 1160  $\text{cm}^{-1}$  in prepared  $\gamma$ -alumina nanoparticles, which belong to symmetrical and asymmetrical  $\text{Al}-\text{O}-\text{H}$  bending modes, respectively. These results are well in accordance with the FTIR spectra of prepared  $\gamma$ -alumina in other researches [35 and 36].





**Figure 7.** FTIR spectra of samples: a) Ab, b) At and c) Ap

#### 4. CONCLUSION

The present study was successful in synthesizing porous  $\gamma$ -alumina nanoparticles by using a facile sol-gel process. The prepared  $\gamma$ -alumina even after calcining the boehmite at 600°C has very high porosity and specific surface area compared with tested commercial  $\gamma$ -alumina sample. Varying the used solvents in the process provided  $\gamma$ -aluminas with relatively high surface area, large pore volume and suitable pore size distribution which are desirable for heavy metal adsorption. The optimum was reached for the At sample with tert-butanol solvent which has a specific surface area of 351 m<sup>2</sup>/g, a pore volume of 1.09 cm<sup>3</sup>/g and particle size of 5.34 nm. This work also shows that the properties of  $\gamma$ -alumina are influenced by the solvent type and important insights on how control textural and structural properties of aluminas, are disclosed.

#### Acknowledgements

The authors gratefully acknowledge from the Material and Energy Research Center (MERC) and the Iranian Nanotechnology Initiative Council for their financial supports of this study.

#### REFERENCES

- [1] Masuda H., Higashitani K., Yoshida H., (2006) Powder Technology: Handling and Operations, *Process Instrumentation and Working Hazards*, CRC Press.
- [2] Jian-hong Y., You-yi S., Jian-feng G., Chun-yan X., (2009) Synthesis of crystalline  $\gamma$ -Al<sub>2</sub>O<sub>3</sub> with high purity, *Transactions of Nonferrous Metals Society of China* 19, 1237-1242.

- [3] Shen S.C., Ng W.K., Chen Q., Zeng X.T., Tan R.B.H., (2007) novel synthesis of lace-like nanoribbons of boehmite and  $\gamma$ -alumina by dry conversion method, *Materials Letters* 61, 4280-4282.
- [4] Liu Y., Ma D., Han X., Bao X., Frandsen W., Wang D., Su D., (2008) Hydrothermal synthesis of microscale boehmite and gamma nanoleaves alumina, *Materials Letters* 62, 1297-1301.
- [5] Lepot N., Van Bael M.K., Van den Rul H., D'Haen J., Peeters R., Franco D., Mullens J., (2008) Synthesis of platelet-shaped boehmite and  $\gamma$ -alumina nanoparticles via an aqueous route, *Ceramics International* 34, 1971-1974.
- [6] Wang S., Li X., Wang S., Li Y., Zhai Y., (2008) Synthesis of  $\gamma$ -alumina via precipitation in ethanol, *Materials Letters* 62, 3552-3554.
- [7] Ma M.G., Zhu J. F., (2009) A facile solvothermal route to synthesis of  $\gamma$ -alumina with bundle-like and flower-like morphologies, *Materials Letters* 63, 881-883.
- [8] Ma M.G., Zhu Y.J., Xu Z.L., (2007) A new route to synthesis of  $\gamma$ -Alumina nanorods, *Materials Letters* 61, 1812-1815.
- [9] Fajardo H.V., Martins A.O., de Almeida R.M., Noda L.K., (2005) Synthesis of mesoporous  $\text{Al}_2\text{O}_3$  microspheres using the biopolymer chitosan as a template: A novel active catalyst system for  $\text{CO}_2$  reforming of methane, *Materials Letters* 59, 3963-3967.
- [10] Haung T.C., Chen H.I., (1995) A STUDY ON THE PREPARATION OF NON-SUPPORTED  $\gamma$ -ALUMINA MEMBRANES BY SOL-GEL METHOD, *Chemical Engineering Communications* 132, 125-139.
- [11] Vallet-Regí M., Rodríguez-Lorenzo L., Ragel C.V., Salinas A.J., González-Calbet J.M., (1997) Control of structural type and particle size in alumina synthesized by the spray pyrolysis method, *Solid State Ionics* Part 1, 197-203.
- [12] Károly Z., Szépvölgyi J., (2003) Hollow alumina microspheres prepared by RF thermal plasma, *Powder Technology* 132, 211-215.
- [13] Chatterjee M., Siladitya B., Naskar M.K., Ganguli D., (2000) sol-emulsion-gel synthesis of alumina nanospheroids, *Trans Indian Ceramic Society* 59, 54-57.
- [14] Ji L., Lin J., Tan K.L., Zeng H.C., (2000) Synthesis of High-Surface-Area Alumina Using Aluminum Tri-sec-butoxide - 2,4-Pentanedione - 2-Propanol - Nitric Acid Precursors, *Chemistry of Materials* 12, 931-939.
- [15] Valente J., Bokhimi X., Toledo J., (2004) Synthesis and catalytic properties of nanostructured aluminas obtained by sol-gel method, *Applied Catalysis A: General* 264, 175-181.
- [16] Kim S.M., Lee Y.J., Bae J.W., Potdar H.S., Jun K.W., (2008) Synthesis and characterization of a highly active alumina catalyst for methanol dehydration to dimethyl ether, *Applied Catalysis A: General* 348, 113-120.
- [17] Huang B., Bartholomew C., Woodfield B.F., (2014) Facile synthesis of mesoporous  $\gamma$ -Alumina with tunable pore size: The effects of water to aluminum molar ratio in hydrolysis of aluminum alkoxides, *Microporous and Mesoporous Materials* 183, 37-47.
- [18] Dabbagh H., Rasti E., Yalfani M., Medina F., (2011) Formation of  $\gamma$ -alumina nanorods in presence of alanine, *Materials Research Bulletin* 46, 271-277.
- [19] Morajkar P., Fernandes J., (2010) A new facile method to synthesize mesoporous  $\gamma$ - $\text{Al}_2\text{O}_3$  of high surface area and catalytic activity, *Catalysis Communications* 11, 414-418.
- [20] Sasani Ghamsari M., Ashor Said Mahzar Z., Radiman S., Abdul Hamid A.M., Rahmani Khalilabad Sh., (2012) Facile route for preparation of highly crystalline  $\gamma$ - $\text{Al}_2\text{O}_3$  nanopowder, *Materials Letters* 72, 32-35.
- [21] Keshavarz A., Rezaei M., Yaripour F., (2011) Preparation of nanocrystalline  $\gamma$ - $\text{Al}_2\text{O}_3$  catalyst using different procedures for methanol dehydration to dimethyl ether, *Natural Gas Chemistry* 20, 334-338.

- [22] Li G., Liu Y., Liu C., (2013) Solvothermal synthesis of gamma aluminas and their structural evolution, *Microporous and Mesoporous Materials* 167, 137-145.
- [23] Brinker C., Scherer G., (1989) Sol–Gel Science, *Academic Press*, New York.
- [24] Cullity B.D., Stock S.R., (2001) Elements of X-Ray Diffraction, *Prentice Hall*, U.S.A.
- [25] Hosseini Z., Taghizadeh M., Yaripour F., (2011) Synthesis of nanocrystalline  $\gamma$ -Al<sub>2</sub>O<sub>3</sub> by sol-gel and precipitation methods for methanol dehydration to dimethyl ether, *Natural Gas Chemistry* 20, 128-134.
- [26] Huang B., Bartholomew C.H., Smith S.J., Woodfield B.F., (2013) Facile solvent-deficient synthesis of mesoporous  $\gamma$ -alumina with controlled pore structures, *Microporous and Mesoporous Materials* 165, 70-78.
- [27] Li G.C., Liu Y.Q., Guan L.L., Hu X.F., Liu C.G., (2012) Meso/macroporous  $\gamma$ -Al<sub>2</sub>O<sub>3</sub> fabricated by thermal decomposition of nanorods ammonium aluminium carbonate hydroxide, *Materials Research Bulletin* 47, 1073-1079.
- [28] Liu X., Peng T., Yao J., Lv H., Huang C., (2010) Synthesis and textural evolution of alumina particles with mesoporous structures, *Solid State Chemistry* 183, 1448-1456.
- [29] Parida K., Pradhan A., Das J., Sahu N., (2009) Synthesis and characterization of nano-sized porous gamma-alumina by control precipitation method, *Materials Chemistry and Physics* 113, 244-248.
- [30] Wang Y., Wang J., Shen M., Wang W., (2009) Synthesis and properties of thermostable  $\gamma$ -alumina prepared by hydrolysis of phosphide aluminum, *Alloys and Compounds* 467, 405-412.
- [31] Huang B., Bartholomew C.H., Woodfield B.F., (2013) Facile structure-controlled synthesis of mesoporous  $\gamma$ -alumina: Effects of alcohols in precursor formation and calcination, *Microporous and Mesoporous Materials* 177, 37-46.
- [32] Lowell S., Shields J. E., (1984) Powder Surface Area and Porosity, *Chapman and Hall*, London and New York.
- [33] Asencios Y.J.O., Sun-Kou M.R., (2012) Synthesis of high-surface-area  $\gamma$ -Al<sub>2</sub>O<sub>3</sub> from aluminum scrap and its use for the adsorption of metals: Pb(II), Cd(II) and Zn(II), *Applied Surface Science* 258, 10002-10011.
- [34] Meephoka C., Chaisuk C., Samparnpiboon P., Praserttham P., (2008) Effect of phase composition between nano  $\gamma$ - and  $\chi$ -Al<sub>2</sub>O<sub>3</sub> on Pt/Al<sub>2</sub>O<sub>3</sub> catalyst in CO oxidation, *Catalysis Communications* 9, 546–550.
- [35] Zeng Z., Yu J., Guo Z.X., (2005) Preparation of functionalized core-shell alumina/polystyrene composite nanoparticles, *Macromolecular Chemistry and Physics* 206, 1558-1567.
- [36] Busca G., Lorenzelli V., Ramis G., Willey R.J., (1993) Surface sites on spinel-type and corundumtype metal oxide powders, *Langmuir* 9, 1492-1499.